Tailoring of thermal expansion and phase transition temperature of ZrW_2O_8 with phosphorus and enhancement of negative thermal expansion of $ZrW_{1.5}P_{0.5}O_{7.75}$

Chenjun Zhang(张晨骏)[1,2], Xiaoke He(何小可)[3,†], Zhiyu Min(闵志宇)[1,2,‡], and Baozhong Li(李保忠)[4]

[1] *School of Agricultural Engineering, Jiangsu University, Zhenjiang* 212013, *China*
[2] *Luoyang Institute of Science and Technology, Luoyang* 471023, *China*
[3] *North China University of Water Resources and Electric Power, Zhengzhou* 450045, *China*
[4] *Luoyang Smart Agricultural Equipment Institute Co., Ltd., Luoyang* 471023, *China*

(Received 28 June 2022; revised manuscript received 2 September 2022; accepted manuscript online 21 September 2022)

ZrW_2O_8 is a typical isotropic negative thermal expansion material with cubic structure. However, quenching preparation, pressure phase transition and metastable structure influence its practical applications. Adopting P to part-substitute W for $ZrW_{2-x}P_xO_{8-0.5x}$ has decreased the sintering temperature and avoided the quenching process. When $x = 0.1$, $ZrW_{1.9}P_{0.1}O_{7.95}$ with a stable cubic structure can be obtained at 1150 °C. The thermal expansion coefficient is tailored with the P content, and phase transition temperature is lowered. When $x = 0.5$, thermal expansion coefficient attains -13.6×10^{-6} °C^{-1}, $ZrW_{1.5}P_{0.5}O_{7.75}$ exhibits enhance negative thermal expansion property. The difference of electronegativity leads to the decrease of phase transition temperature with the increase of P content. The different radii of ions lead to new structure of materials when P substitutes more. The results suggest that the P atom plays the stabilization role in the crystal structure of $ZrW_{2-x}P_xO_{8-0.5x}$.

Keywords: tailored thermal expansion, phase transition, negative thermal expansion, stabilization role, XRD

PACS: 82.47.Aa, 79.60.Jv, 65.40.gk **DOI:** 10.1088/1674-1056/ac9364

1. Introduction

Mismatch in thermal expansion coefficients of different materials can lead to thermal stress and even to failure when temperature changes abruptly. There have many materials which exhibit low and negative thermal expansion (NTE).[1–6] They have been of considerable interest due to potential application in tailoring coefficient of thermal expansion. ZrW_2O_8 is an amazing material because it exhibits a relatively large isotropic negative thermal expansion (NTE) over a wide temperature range of −272.7 °C to 777 °C.[7,8] However, there are some problems in ZrW_2O_8. First, on heating, the structure changes from one cubic phase (α-phase) to another (β-phase) at 180 °C. The coefficient of thermal expansion (CTE) of ZrW_2O_8 is -8.8×10^{-6} °C^{-1}, and -4.9×10^{-6} °C^{-1} for α-phase and β-phase ZrW_2O_8. Second, the cubic phase α-ZrW_2O_8 will transform to the orthorhombic phase γ-ZrW_2O_8 under low pressure (0.27 GPa).[9,10] Third, hydration of ZrW_2O_8 gives the monohydrate ZrW_2O_8–H_2O, which has a molar volume 10% smaller than ZrW_2O_8.[11] NET only appears after the loss of crystal water. However, cubic phase ZrW_2O_8 is a metastable phase at room temperature needing quenching preparation, which is prone to temperature and pressure phase transition and decomposition.

Ion substitution can change the phase transition and the thermal expansion coefficient of the material. $ZrW_{2-x}V_xO_{8-x/2}$ and $Zr(W_{1-y}Mo_y)_{2-x}V_xO_{8-x/2}$ have been reported with negative thermal expansion property by using the substitutions V and/or Mo for W in ZrW_2O_8.[12–14] However, tailored thermal expansion phenomenon is not obvious, which could be related to the NTE of ZrV_2O_7.[15] ZrP_2O_7 with similar cubic phase at room temperature to ZrV_2O_7 could be a better candidate due to its positive thermal expansion property.[16] Dual-ion substitutions of Cu^{2+}/P^{5+} or Fe^{3+}/P^{5+} for Zr^{4+}/V^{5+} in ZrV_2O_7 have been reported.[17,18] However, it is difficult to reach a high solubility of the dopants in ZrV_2O_7.

To obtain a stable NTE material, $A_2M_3O_{12}$ (A represents trivalent metals such as Y, Yb, In, Fe, and Al) is a good choice. The framework structures of $A_2M_3O_{12}$ are composed of MO_4 tetrahedron and AO_6 octahedron. $Zr_2WP_2O_{12}$ could be a typical example for obtaining novel NTE material, however, the NTE coefficient is only about -2.61×10^{-6} K^{-1}.[19] Isobe *et al.* sintered $Zr_2WP_2O_{12}$ with more than 0.5 wt% MgO, the NTE coefficient is only about -3.4×10^{-6} K^{-1}.[20] $Zr_2W_2P_2O_{15}$ exhibits the NTE property with larger CTE.[21] On the other hand, the orthorhombic-cubic phase transition temperature of $Zr(W_{1-y}Mo_y)_{2-x}V_xO_{8-x/2}$ decreases linearly with increasing V content.[12,13] The phase transition temperature (from α-phase to β-phase) of $ZrW_{2-x}V_xO_{8-x/2}$ decreases linearly with increasing V content. When $x \geq 0.29$, $ZrW_{2-x}V_xO_{8-0.5x}$ is β-phase at room temperature.[14] Light-

†Corresponding author. E-mail: hexiaoke@ncwu.edu.cn
‡Corresponding author. E-mail: 200900300185@lit.edu.cn

© 2023 Chinese Physical Society and IOP Publishing Ltd

weight zero-thermal expansion materials were developed by ZrW_2O_8 and SiCnw/Al (nw: nano wire).[22] It is predictable that the P substitution for W in ZrW_2O_8 could decrease the phase transition temperature.

In this work, $ZrW_{2-x}P_xO_{8-0.5x}$ solid solutions are developed by the solid state method with substitution of P^{5+} for W^{6+}. The sintering temperature is decreased and the quenching process is avoided. With increasing the P content, the CETs of the samples are tailored, and phase transition temperature is lowered.

2. Materials and methods

$ZrW_{2-x}P_xO_{8-0.5x}$ was synthesized by solid state method from WO_3, ZrO_2 and P_2O_5. The raw materials were mixed according to the stoichiometric ratios of destination materials and ground in a mortar for 3 h, put into dry box at 140 °C for 10 h, and then pressed into tablets with length about 10 mm and diameter 10 mm followed by sintering at 1150 °C for 2 h ($x = 0.1$ and 0.2), and 1100 °C for 2 h ($x \geq 0.3$), finally cooled down in furnace naturally.

X-ray diffraction (XRD) measurements were carried out with an X'Pert PRO x-ray diffractometer. Raman spectroscopy (Renishaw MR-2000 Raman spectrometer) was used to characterize the vibrational property of lattice. The linear thermal expansion coefficients of the samples were measured by employing a dilatometer (LINSEIS DIL L76), with the heating and cooling rates of 5 °C/min.

3. Results and discussion

Figure 1 shows the XRD patterns of prepared $ZrW_{2-x}P_xO_{8-0.5x}$. When $x = 0.0$, the primary diffraction peaks are corresponding to ZrW_2O_8 (JCPDF card: 01-089-6670). When $x = 0.1$ (see Fig. 1(a)), the primary diffraction peaks are corresponding to $x = 0.0$, which indicates that $ZrW_{1.9}P_{0.1}O_{7.95}$ with cubic structure is successfully obtained. We can obtain pure phase with cubic structure at lower temperature of 1150 °C, which reduces the energy loss of preparing cubic phase zirconium tungstate. However, comparing the diffraction peaks of the samples with $x = 0.0$ and 0.2, we can observe that there is the secondary phase in $x = 0.2$ (see Fig. 1(b)). From $x = 0.2$ to $x = 0.5$, the relative intensity of main diffraction peak at about either 21.8° remains strongest diffraction peak, or 23.8° is secondary main peak the primary peaks still remain that of $x = 0$, indicating that the primary structure is the same crystal structure (cubic structure) as that of ZrW_2O_8. The characteristic peak Miller index corresponding to a thought at around 31° is 310, which is always present at room temperature. This means that materials are α-phase. The strongest diffraction peak at about 21.8° continues to weaken, the secondary peak becomes stronger and it becomes strongest diffraction peak when $x \geq 0.6$. Some new diffraction peaks appear at about 12°, 15°, 20°, 22.5°, 23.5°, and 24.5°. They emerge with further increasing substitution amounts of P^{5+} from $x = 0.6$ to $x = 0.9$. At the same time, the peaks at 16.0° and 19.4° disappear. The XRD result shows that the symmetry of crystal lattice changes from cubic to orthorhombic or monoclinic structure with increasing the substitutions of P^{5+} for W^{6+}.

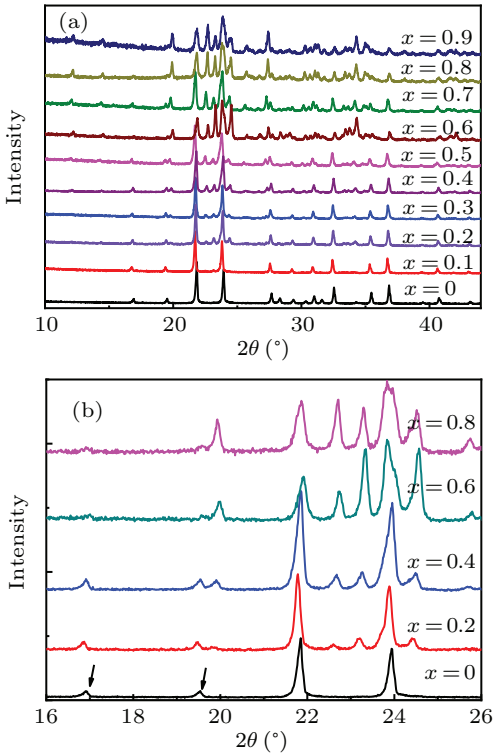


Fig. 1. XRD patterns of $ZrW_{2-x}P_xO_{8-0.5x}$ with $x = 0$, 0.1, 0.2, 0.3, 0.5, 0.6, 0.7, 0.8, and 0.9.

Figure 2(a) is a comparison diagram of the XRD patterns of $x = 0.1$ and the JCDPDF card (083-1005). It is obvious that the sample of P-doped ZrW_2O_8 presents basically the same structure as that of ZrW_2O_8 (PDF No. 01-083-1005, space group: $Pa\bar{3}$). The shifts of the peaks suggest a decrease in lattice constant and this is confirmed by lattice constant calculations as shown in Fig. 1. Figure 2(b) shows that the lattice constant decreases successively with increasing the content of P. The lattice constants are determined using about 32 diffraction peaks between 10° and 80° by a least-square method after correcting 2θ. The lattice constant decreases from 0.915 nm to 0.913 nm as the P substitution increases. The decrease in lattice constant is attributed to the introduction of the radius of P^{5+} (38 pm) smaller than that of W^{6+} (62 pm). Figure 2(c) is a comparison diagram of the XRD patterns of $x = 0.8$ and the JCDPDF card (089-2239). It is obvious that the sample of P-doped ZrW_2O_8 presents basically the same structure as that of $Zr_2WP_2O_{12}$ (PDF No. 01-089-2239, space group: *Pnca*), which indicates the $ZrW_{1.2}P_{0.8}O_{7.6}$ crystals in the orthorhombic structure.

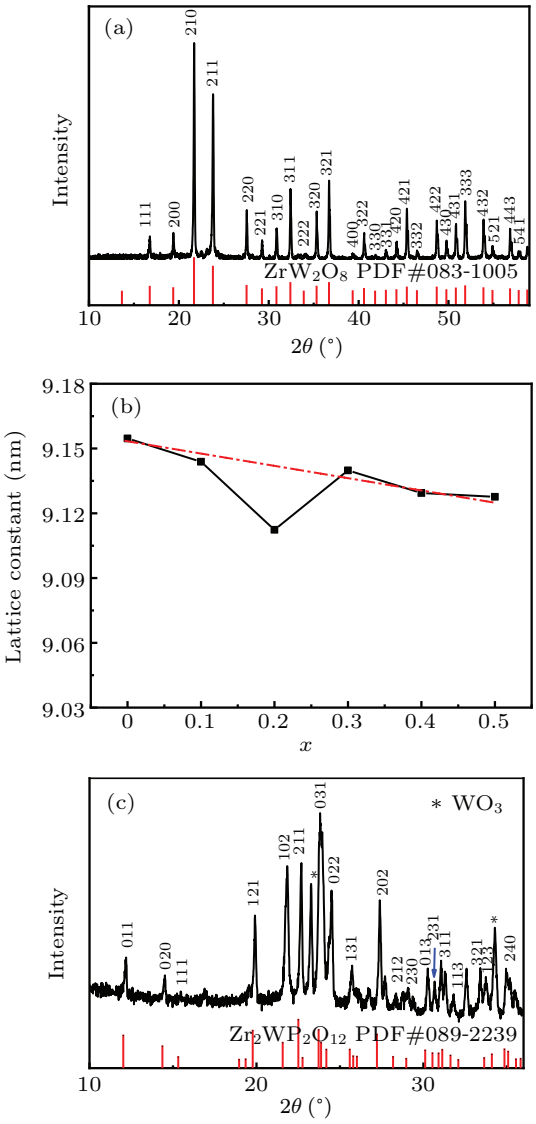


Fig. 2. (a) XRD patterns of $ZrW_{1.9}P_{0.1}O_{7.95}$ and XRD peaks of JCDPDF #01-083-1005. (b) Dependence of the lattice constants of P-doped ZrW_2O_8 on the value of x. (c) XRD patterns of $ZrW_{1.2}P_{0.8}O_{7.6}$ and XRD peaks of JCDPDF #01-089-2239.

Figure 3 shows the Raman spectra of the as-prepared $ZrW_{2-x}P_xO_{8-0.5x}$. All Raman peaks could be considered to be caused by stretching and bending vibrations of PO_4 and WO_4 tetrahedrons.[16–20] When $x = 0$, the Raman spectra agree with the previous report,[16] which means that the sample is pure ZrW_2O_8. The peaks at about 1028 cm^{-1}, 929 cm^{-1}, and 900 cm^{-1} could be referred as symmetric stretching ($\nu 1$) of the WO_4 tetrahedra. The peaks at about 788 cm^{-1} and 734 cm^{-1} could be referred as asymmetric stretching ($\nu 3$) of the WO_4 tetrahedra. Bending ($\nu 2 + \nu 4$) vibrations of the WO_4 tetrahedra falls in the regions of 200–400 cm^{-1}. The lower wavenumber bands are external modes from lattice, translational and librational motions.[17] There are few changes with the addition of P first ($x \leq 0.5$), except that there appear new Raman peaks at about 868 cm^{-1} and 1019 cm^{-1}, however stretching of the PO_4 tetrahedra is not found. This is due to the lattice strain caused by the addition of P. These phenomena illustrate that the materials remain the cubic structure of ZrW_2O_8.

When $x \geq 0.6$, some new peaks at about 1095 cm^{-1}, 1037 cm^{-1}, 1019 cm^{-1}, and 824 cm^{-1} emerge and other peaks at about 1028 cm^{-1}, 929 cm^{-1}, 900 cm^{-1}, 788 cm^{-1}, and 734 cm^{-1} disappear at high wave numbers. By comparison with Raman spectra of other compounds with the general formula $A_2M_3O_{12}$[17,18] and ZrW_2O_8, these new modes at about 1095 cm^{-1}, 1037 cm^{-1}, 1019 cm^{-1}, and 824 cm^{-1} vibrations can be classified as stretching of the WO_4 and PO_4 tetrahedra in $Zr_2WP_2O_{12}$,[16,19,20] and 250 cm^{-1}, 303 cm^{-1}, 315 cm^{-1}, 346 cm^{-1}, 408 cm^{-1}, and 427 cm^{-1} can be classified as bending of the WO_4 and PO_4. The disappearance of the characteristic vibration peaks indicates that the cubic phase no longer exists. The phenomena indicate that there is phase transition caused by the large amount of P substitution. The Raman spectra of materials are similar with $Zr_2WP_2O_{12}$.[21] These indicate that the structure of $Zr_2WP_2O_{12}$ is orthorhombic at room temperature. It can be indicated that the materials crystalize in orthorhombic structure. The result agrees with the result of XRD.

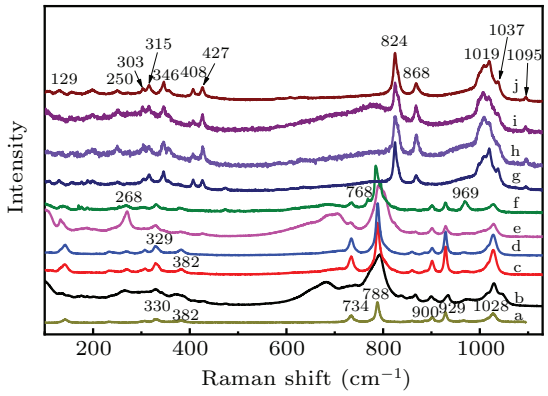


Fig. 3. Raman spectra of $ZrW_{2-x}P_xO_{8-0.5x}$ with $x = 0$, 0.1, 0.2, 0.3, 0.5, 0.6, 0.7, 0.8, and 0.9 (a–j).

In order further to check the effect of the substitution of P for W of ZrW_2O_8, the microstructures of $ZrW_{2-x}P_xO_{8-0.5x}$ are performed by SEM (Figs. 4(a)–4(d) for $x = 0.2$, 0.5, 0.6, and 0.9, respectively). For $x = 0.2$, the SEM image shows that the materials are composed of almost homogeneous particles in the grain size of about 4–8 μm, and there are few holes and the structure is dense (Fig. 4(a)). This means that the material has good consistency and uniformity. The same result EDS is obtained by the energy dispersive spectroscopy (EDS) spectrum analysis and elemental mapping grains [Fig. 4(e)]. For $x = 0.5$, the grain size is no longer uniform. However, microstructure comprises regular shaped particles with clear boundaries, smooth surface. The result of EDS of $ZrW_{1.5}P_{0.5}O_{7.75}$ (Fig. 4(f)) indicates that various elements are evenly distributed. The structure of $ZrW_{2-x}P_xO_{8-0.5x}$ ($x \leq 0.5$) is a framework of corner-sharing

ZrO_6 octahedra and WO_4 (or PO_4) tetrahedra. The octahedra share all their six corners with different six WO_4 tetrahedra while WO_4 tetrahedra share only three of their four oxygens with the neighboring ZrO_6 octahedra. This would make the materials to crystalize in cubic structure (Figs. 4(a) and 4(b)). The results of XRD and Raman reach the same conclusion. However, increase of P ($x \geq 0.6$) will strengthen the lattice distortion because of the difference of lattice radius of W^{6+} and P^{5+}. For $x = 0.6$ and 0.9, the material is no longer composed of regular particles, but of irregular rock-like structure with sharp corners. This is because the crystal structure of the material has changed. The results agree with the data of XRD and Raman spectra.

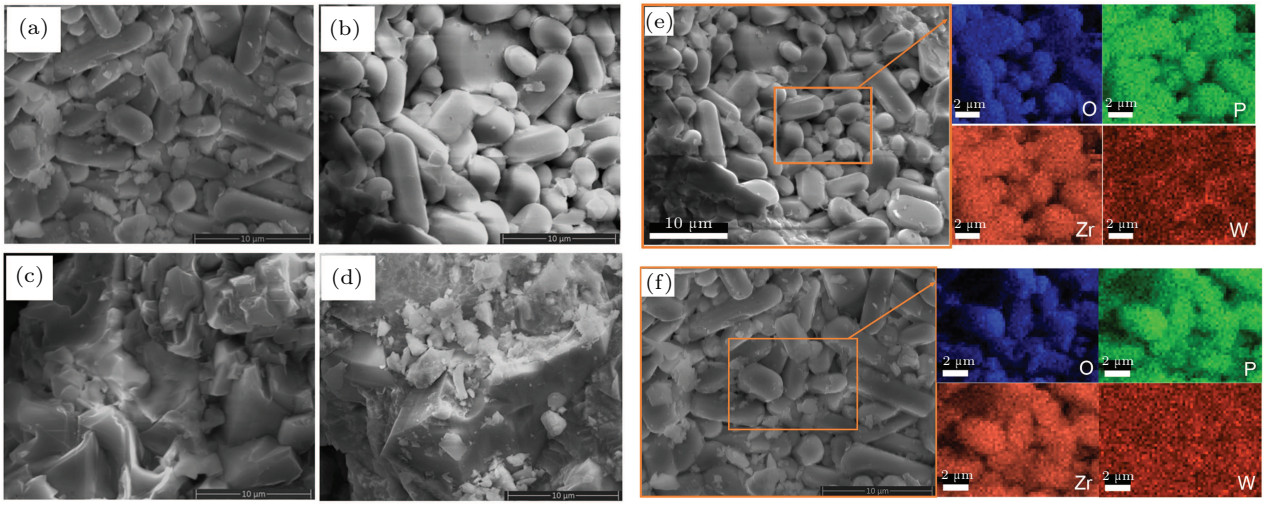


Fig. 4. (a)–(d) SEM image of $ZrW_{2-x}P_xO_{8-0.5x}$ with $x = 0.2$, 0.5, 0.6, 0.9 and (e), (f) EDS mapping for $x = 0.2$ and 0.5.

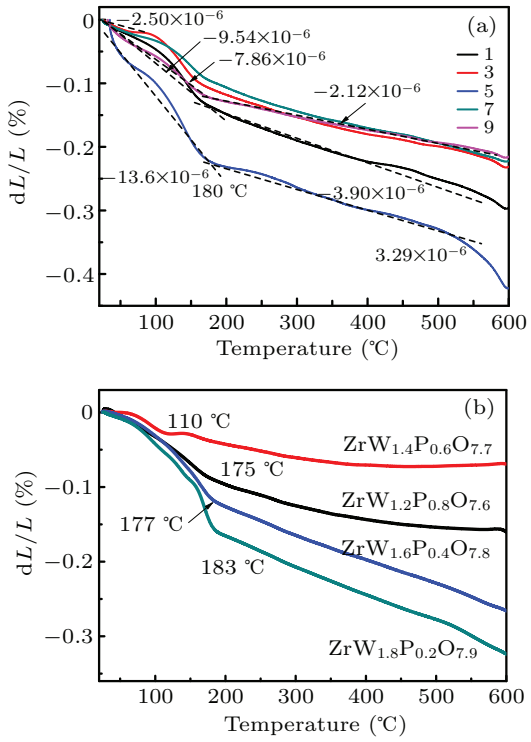


Fig. 5. Relative length change versus temperature with (a) $x = 0.1$, 0.3, 0.5, 0.7, 0.9, and (b) $x = 0.2$, 0.4, 0.6 and 0.8.

Figure 5 shows the relative length changes of $ZrW_{2-x}P_xO_{8-0.5x}$ with $x = 0.1$, 0.3, 0.5, 0.7, and 0.9, $x = 0.2$, 0.4, 0.6 and 0.8, respectively, obtained from dilatometer. It is found that the samples prepared with different P contents have different relative linear thermal expansions. Phase transition temperature is related with P content, which means that P can affect both thermal expansion and phase transition temperature of materials. We can see that phase transition temperature decreases with the increase of P content, meanwhile the thermal expansion coefficients of materials before and after phase transformation are inhibited with the increase of P content. However, when $x = 0.5$, there is an abnormal phenomenon. The thermal expansion coefficient attains -13.6×10^{-6} K^{-1} before phase transformation. This is higher than that of ZrW_2O_8. The thermal expansion coefficient attains -3.29×10^{-6} K^{-1} after phase transformation, which is much lower than that of ZrW_2O_8. The phase transition temperature of $x = 0.1$, 0.2, 0.3, 0.4, and 0.5 are 163 °C, 183 °C, 160 °C, 177 °C, and 180 °C, respectively. It can be found that thermal expansion coefficients decrease with the increase of P content, especially for $x = 0.8$ and 0.9 the thermal expansion coefficients are about -2.12×10^{-6} K^{-1}, which is close to $Zr_2WP_2O_{12}$. These means that a large content of P leads to the change of material structure.

For ZrW_2O_8 (Fig. 5), there are two turning points corresponding to two phase transitions from α-phase to β-phase and unknown phase transition. ZrW_2O_8 presents lower NTE property after the latter phase transition. For $ZrW_{1.5}P_{0.5}O_{7.5}$ (Fig. 4), only one turning point is observed and the thermal contraction is strengthened. The electronegativity of P is higher than that of W, the bond strength of W–O is higher than P–O, phase transition absorbs less energy, and phase transi-

tion temperature is lower than ZrW_2O_8 (see Fig. 5). However, ionic radius of P^{5+} (38 pm) is less than that of W^{6+} (60 pm), this could lead to that atomic space occupancy decrease when P content is low ($x \leq 0.5$). With increasing the content of P, the coefficients of thermal expansion below the turning temperature are remarkably further suppressed, suggesting that the latter phase transition is largely suppressed. P-doped ZrW_2O_8 samples with $x = 0.8$ and 0.9 present low thermal expansion without turning point. The bond length of P–O is shorter than W–O, lattice distortion could occur with the increase of P content ($x \geq 0.6$) (see Fig. 1) and the Coulomb interaction between ions is larger, which lead to lower thermal expansion coefficient (see Fig. 5).

4. Conclusions

New serial NTE materials of $ZrW_{2-x}P_xO_{8-0.5x}$ are prepared with the solid state method. The phase transition temperature and thermal expansion coefficient are influenced by the P content. It is found that materials remain cubic structure when $x \leq 0.5$, and change to orthorhombic structure when $x \geq 0.6$. When $x = 0.1$, $ZrW_{1.9}P_{0.1}O_{7.95}$ with a stable cubic structure can be obtained at 1150 °C. The thermal expansion coefficient attains -13.6×10^{-6} K^{-1} before phase transformation when $x = 0.5$, which is higher than that of ZrW_2O_8. The phase transition temperature is 110 °C when $x = 0.6$. When $x = 0.8$, 0.9, the structure and thermal expansion are close to $Zr_2WP_2O_{12}$ except that there is phase transformation at about 140 °C.

Acknowledgement

Project supported by the Key Scientific and Technological Research Projects of Henan Province, China (Grant Nos. 222102220021 and 222102220056).

References

[1] Chen J, Wang F F, Huang Q Z, Hu L, Song X P, Deng J X, Yu R B and Xing X R 2013 *Sci. Rep.* **3** 2458
[2] Curry E B, Lyszak K, Sheets D, Occhialini C A, Rozman M G and Hancock J N 2021 *Front. Mater.* **22** 742195
[3] Bird T A, Woodland-Scott J, Hu L, Wharmby M T, Chen J, Goodwin A L and Senn M S 2020 *Phys. Rev. B* **101** 064306
[4] Shuitcev A, Vasin R N, Balagurov A M, Li L, Bobrikov I A and Tong Y X 2020 *Intermetallics* **125** 106889
[5] Yuan H L, Gao Q L, Xu P, Guo J, He L H, Sanson A, Chao M J and Liang E J 2021 *Inorg. Chem.* **60** 1499
[6] Toshihiro I, Yuko H, Yuri A, Ryosuke U, Sachiko M and Akira N 2020 *NPG Asia Mater.* **12** 80
[7] Mary T A, Evans J S O, Vogt T and Sleight A W 1996 *Science* **272** 90
[8] Evans J S O, Mary T A, Vogt T, Subramanian M A and Sleight A W 1996 *Chem. Mater.* **8** 2809
[9] Perottoni C A and Jornada A H 1998 *Science* **280** 886
[10] Hashimoto T, Katsube T and Morito Y 2000 *Solid State Commun.* **116** 129
[11] Banek N A, Baiz H I, Latigo A and Lind C 2012 *J. Am. Chem. Soc.* **132** 8278
[12] Chen X, Guo F L, Deng X B, Tao J Z, Qin D L and Zhao X H 2014 *J. Alloys Compd.* **612** 252
[13] Chen X, Guo F L, Deng X B, Tao J Z, Ma H and Zhao X H 2012 *J. Alloys Compd.* **537** 227
[14] Chen X, Deng X B, Ma H, Tao J Z and Zhao X H 2011 *J. Solid State Chem.* **184** 1090
[15] Petruska E A, Muthu D V S, Carlson S, Krogh Andersen A M, Ouyang L and Kruger M B 2010 *Solid State Commun.* **150** 235
[16] Liang E J, Liang Y, Zhao Y, Liu J and Jiang Y J 2008 *J. Phys. Chem. A* **112** 12582
[17] Yuan B H, Yuan H L, Song W B, Liu X S, Cheng Y G, Chao M J and Liang E J 2014 *Chin. Phys. Lett.* **31** 076501
[18] Yuan B H, Liu X S, Song W B, Cheng Y G, Liang E J and Chao M J 2014 *Phys. Lett. A* **378** 3397
[19] Liu X S, Wang J Q, Fan C Z, Shang R, Cheng F X, Yuan B H, Song W B, Cheng Y G, Liang E J and Chao M J 2015 *Int. J. Appl. Ceram. Technol.* **12** E28
[20] Isobe T, Umezome T, Kameshima Y, Nakajima A and Okada K 2009 *Mater. Res. Bull.* **44** 2045
[21] Yuan B H, Chen Y G, Zhang Q L, Chen L L and Liu X S 2017 *Ceram. Inter.* **43** 6831
[22] Zhou C, Zhou Y X, Liu S Y, Zhang L Y, Song P Y, Zhang Q, Ma B Y and Wu G H 2022 *J. Alloys Compd.* **907** 164444